

The critical role of Ru-like hydrogen adsorption of carbon dots in carbon confined Ru system for a boosted HER activity

Zonglin Liu^a, Honglei Zhang^a, Dongyue Liu^a, Yujie Feng^a, Dechang Jia^a, Caicai Li^{c,*},
Qingfeng Sun^c, Yu Zhou^a, Zhenhui Kang^{d,*}, Baoqiang Li^{a,b,e*}

^a Institute for Advanced Ceramics, State Key Laboratory of Urban Water Resource and Environment, Harbin Institute of Technology, Harbin 150001, China

^b School of Engineering, Zhejiang A & F University, Hangzhou, 311300, China

^c Laboratory of Dynamics and Extreme Characteristics of Promising Nanostructured Materials, Saint Petersburg State University, St. Petersburg, 199034, Russia

^d Institute of Functional Nano and Soft Materials (FUNSOM), Jiangsu Key Laboratory for Carbon-Based Functional Materials and Devices, Soochow University, Suzhou, 215123, China

^e MIIT Key Laboratory of Advanced Structural-Functional Integration Materials & Green Manufacturing Technology, Harbin Institute of Technology, Harbin 150001, China

*Correspondence and requests for materials should be addressed to Baoqiang Li (email: libq@hit.edu.cn), Caicai Li (email: ccli@zafu.edu.cn) and Zhenhui Kang (email: zhkang@suda.edu.cn).

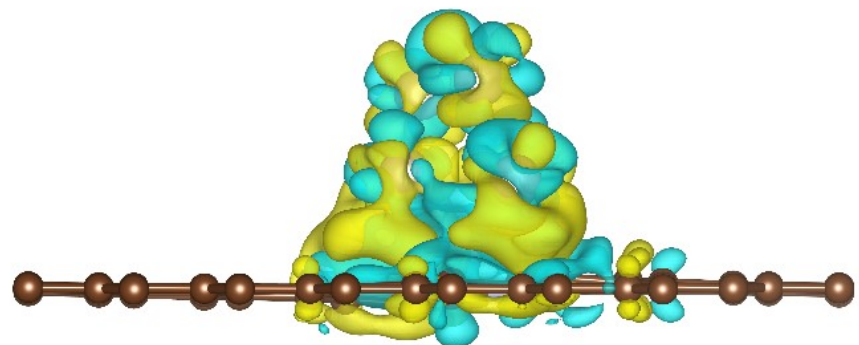


Figure S1. Electron density difference map of Ru/NCDs, where a loss of electrons is indicated in blue, and electron enrichment is indicated in yellow.

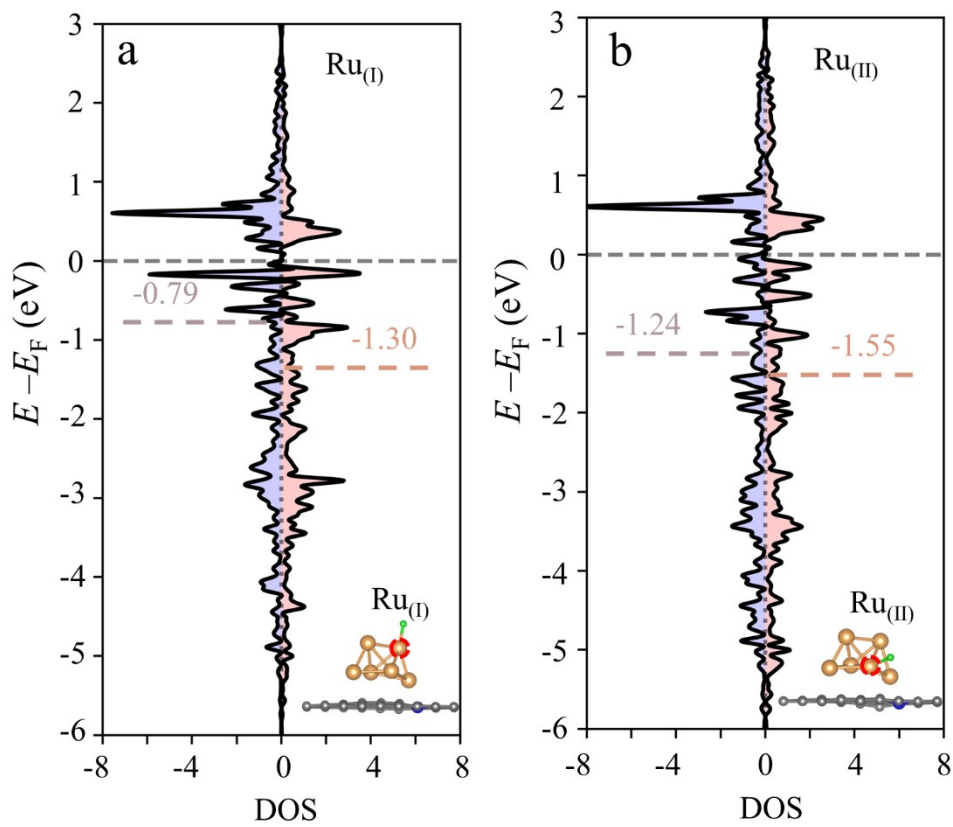


Figure S2. The DOS plots of (a) Ru_(I) at the top and (b) Ru_(II) at the interface, the position of the center of the d-band is marked by a dashed line.

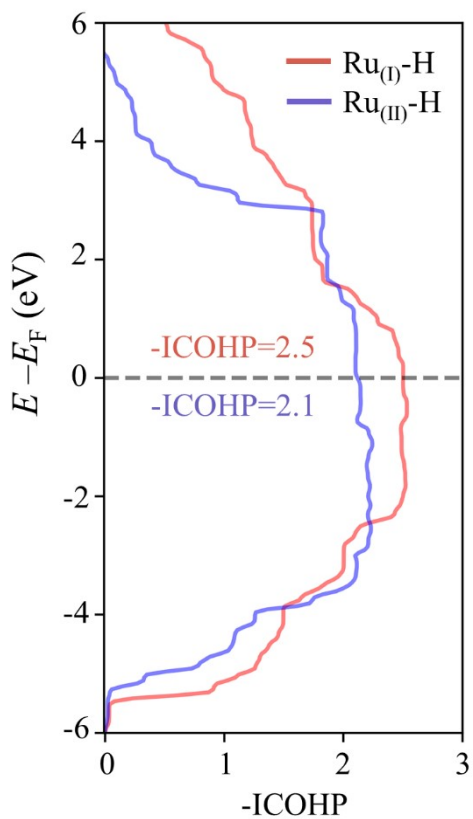


Figure S3. The corresponding ICOHP of $\text{Ru}_{(\text{I})}$ at the top and $\text{Ru}_{(\text{II})}$ at the interface.

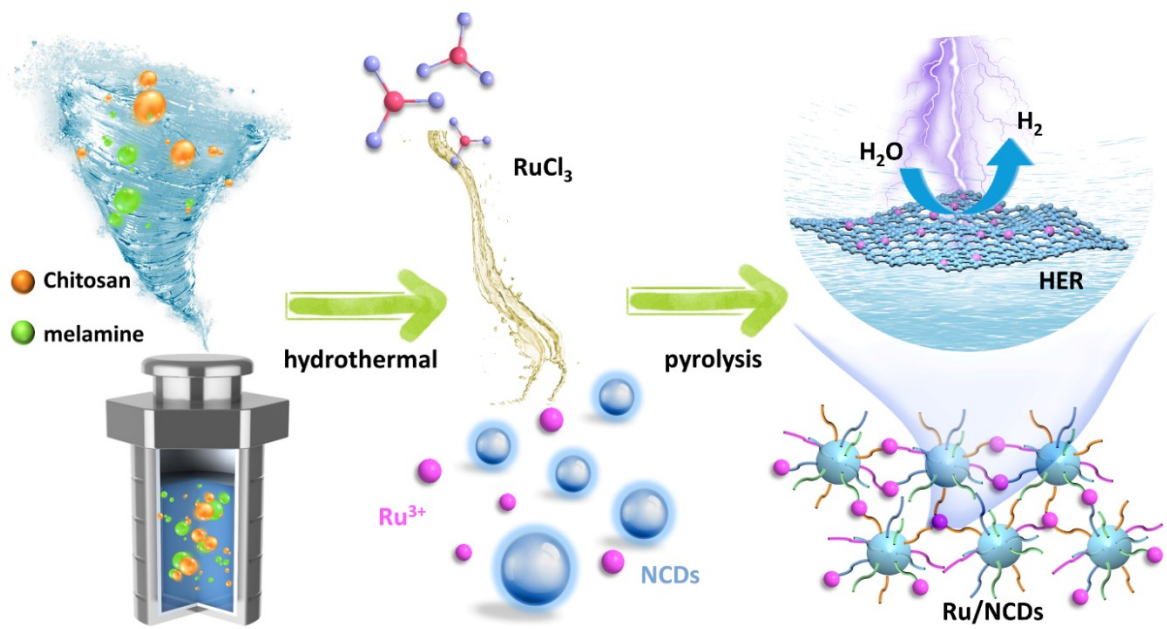


Figure S4. Schematic illustration for the synthesis of Ru/NCDs.

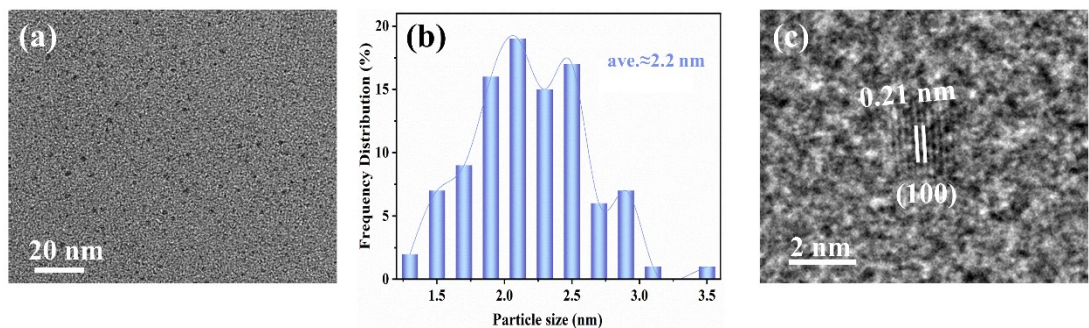


Figure S5. (a) Low-magnified TEM image of NCDs. (b) Size distribution histogram of NCDs. (c) HRTEM images of NCDs.

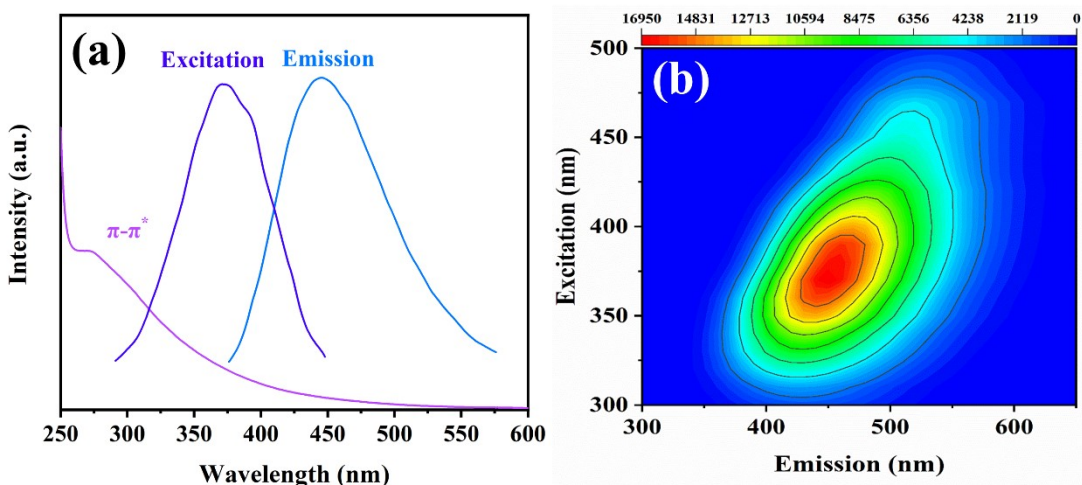


Figure S6. (a) UV-vis, PL excitation, and PL emission spectra of NCDs. (b) Excitation–emission matrix of NCDs. The UV-vis spectrum of the NCDs presents an absorption peak in the range of 250 ~ 300 nm, which is caused by the $\pi-\pi^*$ transition of aromatic C=C bonds. According to photoluminescence experiments, the maximum excitation wavelength and emission wavelength of NCDs are 370 and 445 nm, respectively.

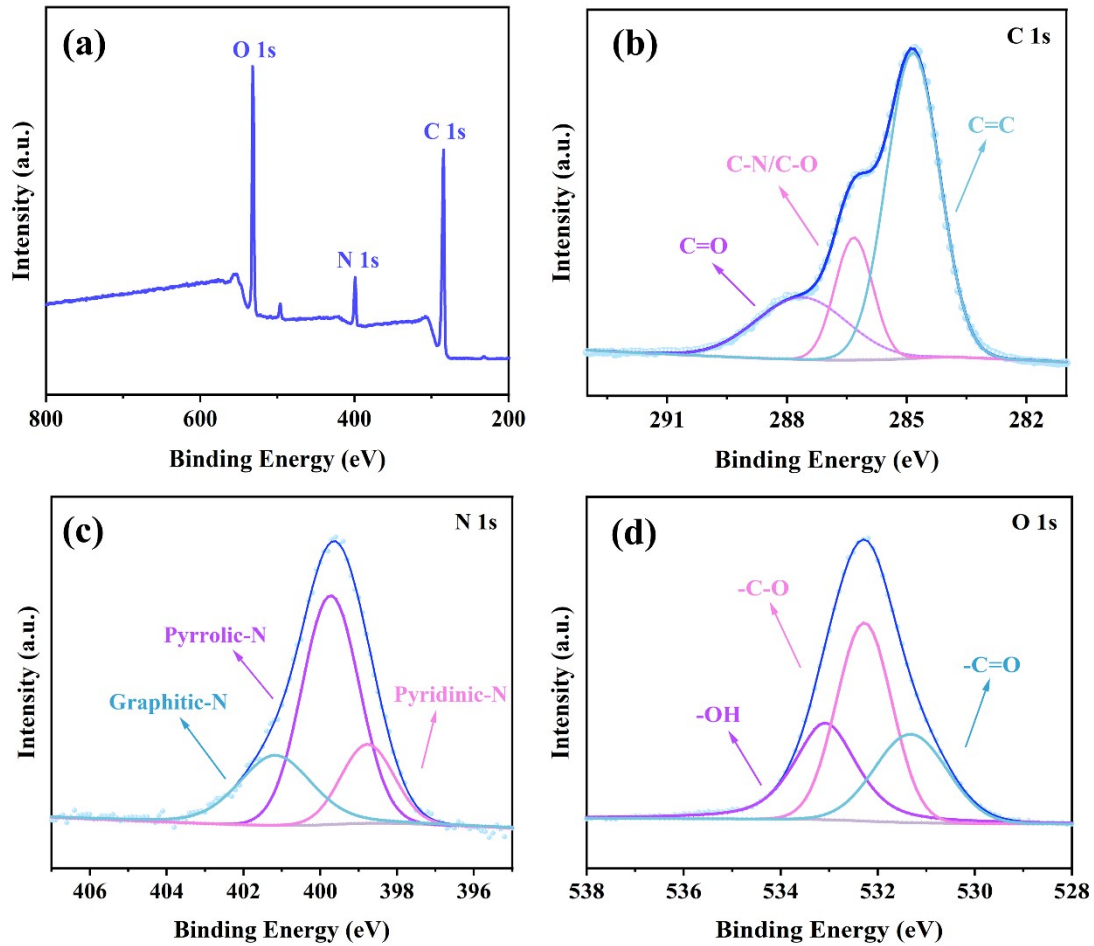


Figure S7. (a) XPS survey scan of NCDs. (b) High-resolution XPS spectra of C 1s of NCDs. In the high-resolution XPS spectra of C 1s, three separated peaks centered at 287.6 eV (C=O bond), 286.3 eV (C-N/C-O bond), and 284.8 eV (C=C bonds) are observed. (c) High-resolution XPS spectra of N 1s of NCDs. The three peaks in the high-resolution N 1s spectrum are ascribed to graphitic N (401.2 eV) pyrrolic N (399.7 eV) and pyridinic N (398.7 eV). High-resolution XPS spectra of O 1s of NCDs. O 1s spectra can be deconvoluted into three peaks, and the peaks at 533.1, 532.3, and 531.3 eV are attributed to the -OH, -C-O, and -C=O, respectively.

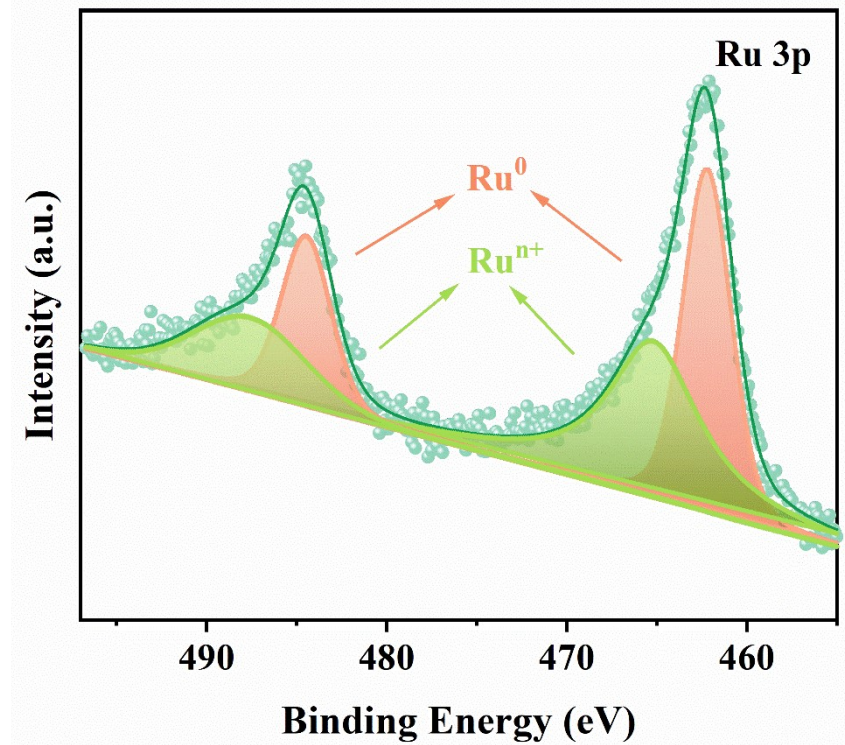


Figure S8. High-resolution XPS spectrum of Ru 3p of Ru/NCDs.

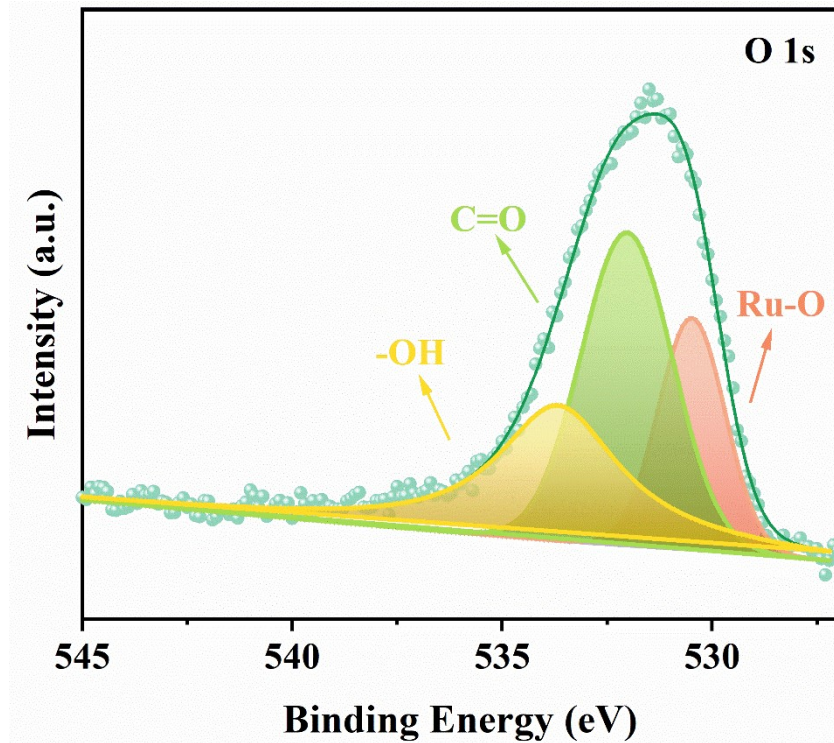


Figure S9. High-resolution XPS spectrum of O 1s of Ru/NCDs. The peaks at 533.7, 532.0 and 530.5 eV in the high-resolution O 1s spectra are part of the -OH, -C=O and Ru-O bonds of Ru/NCDs, which proves that the Ru/NCDs are rich in functional groups on the surface and the Ru nanoparticles are tightly connected to the NCDs.

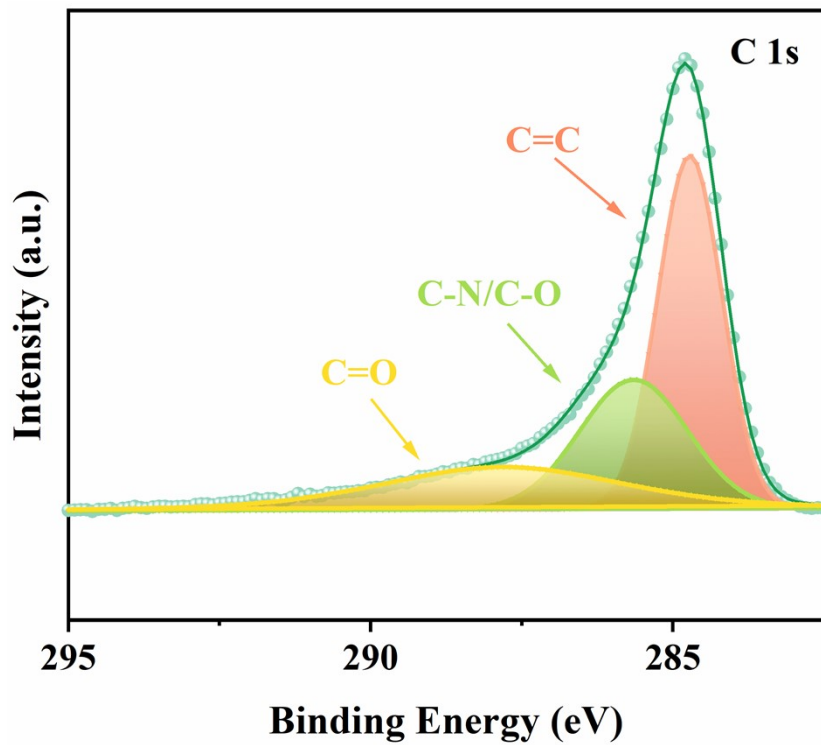


Figure S10. High-resolution XPS spectrum of C 1s of Ru/NCDs. The binding energies located at 287.8, 285.6 and 284.7 eV correspond to the C=O, C-N/C-O and C=C bond, respectively.

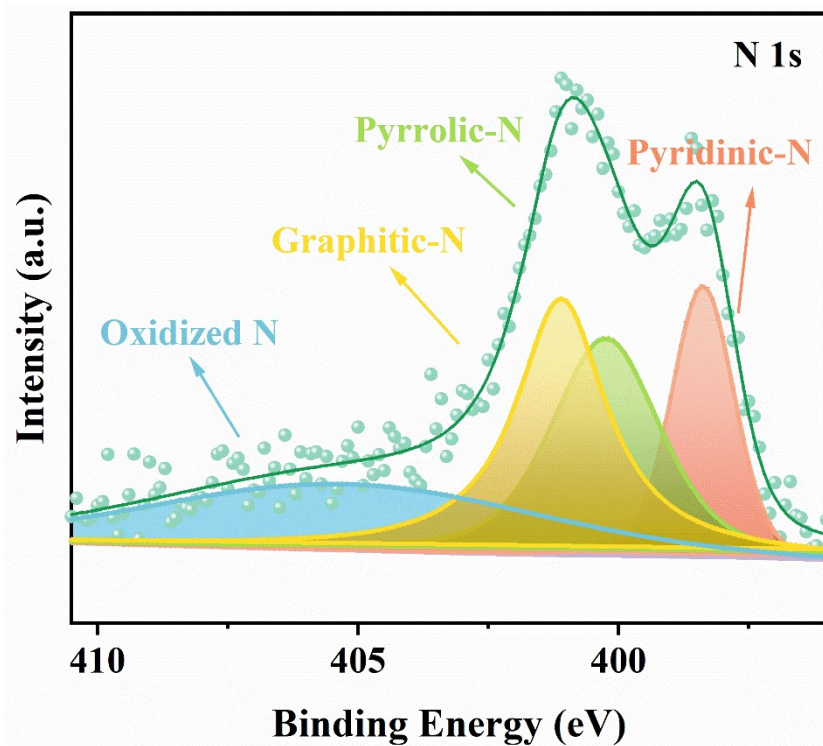


Figure S11. High-resolution XPS spectrum of N 1s of Ru/NCDs. The binding energies of N element appearing at 405.5, 401.1, 400.3 and 398.4 eV correspond to the oxidized N, graphitic N, pyrrolic N and pyridinic N, respectively.

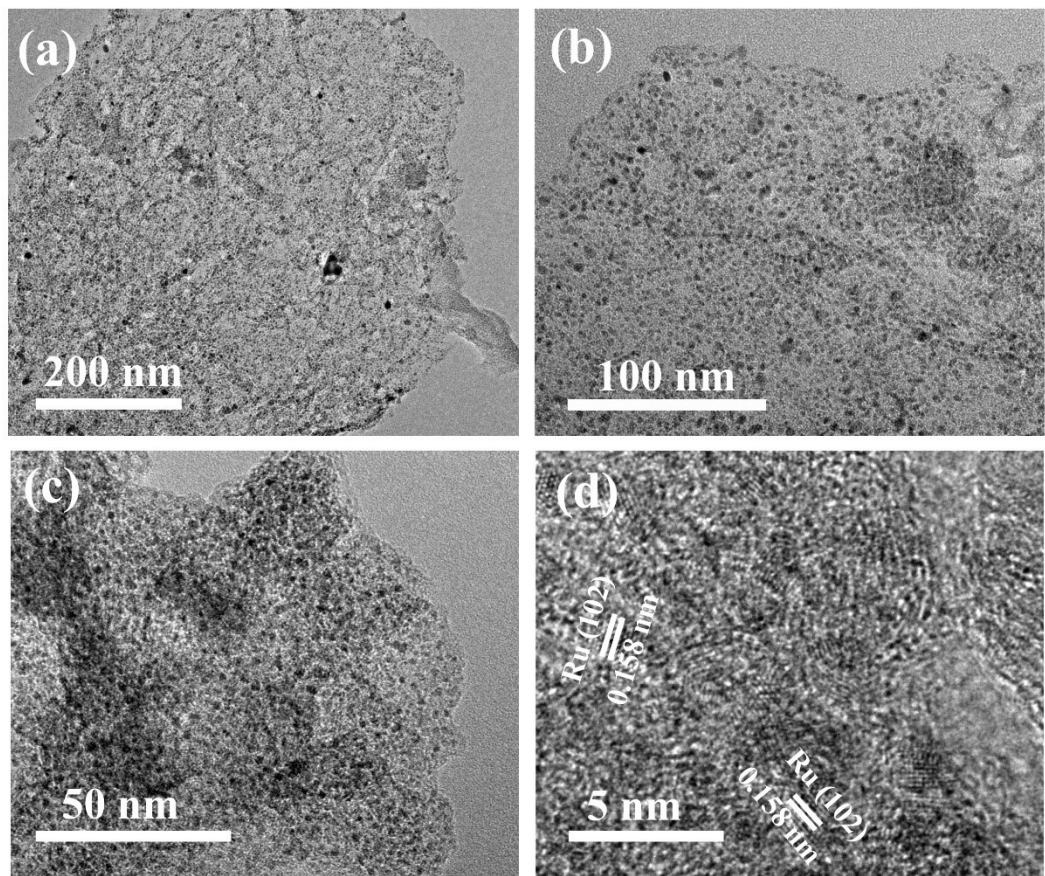


Figure S12. TEM images of Ru/NCDs under different magnifications.

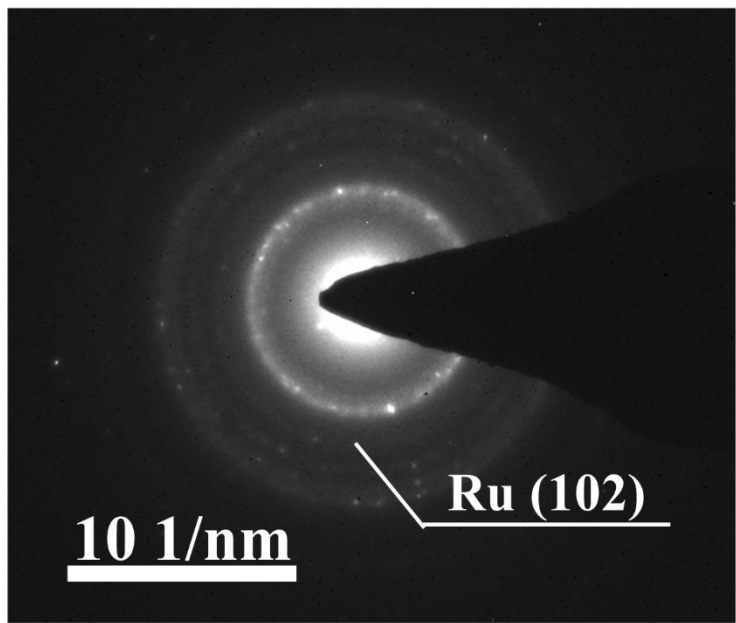


Figure S13. The SEAD pattern recorded from the corresponding area.

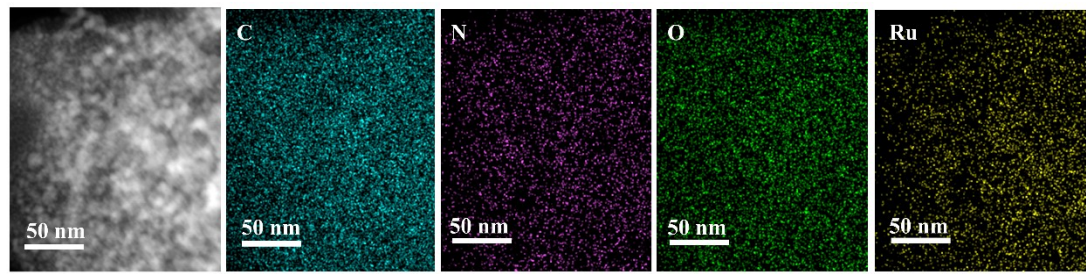


Figure S14. HAADF-STEM image and elemental mapping of C, N, O and Ru in Ru/NCDs.

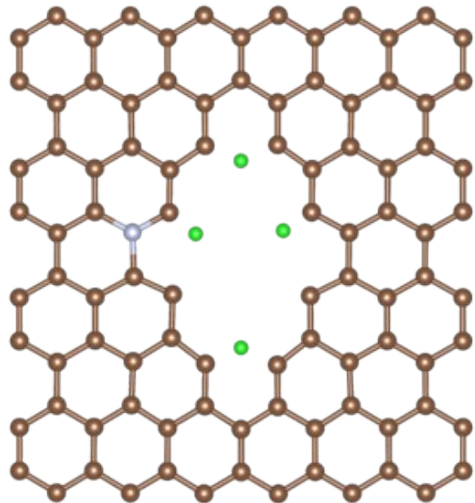


Figure S15. The configuration of adsorbing hydrogen atoms in the gaps of the carbon substrate. The configuration of adsorbing hydrogen atoms in the gaps of the carbon substrate is shown in the figure below, in which some carbon atoms are removed from graphene to simulate the gaps in the carbon substrate. An appropriate amount of hydrogen atoms was absorbed on the gap, and the average adsorption energy of hydrogen atoms was calculated by the following formula :

$$E_{avg} = \frac{E_t}{n}$$

Among them, E_{avg} is the average adsorption energy, E_t is the total adsorption energy of multiple hydrogen atoms, n is the number of hydrogen atoms adsorbed.

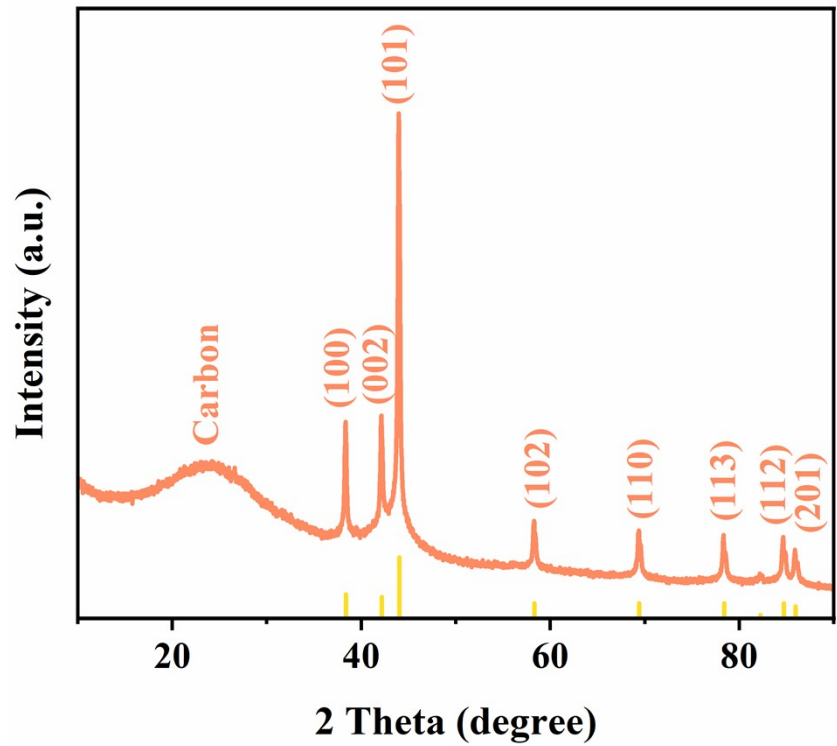


Figure S16. XRD pattern of Ru/NC.

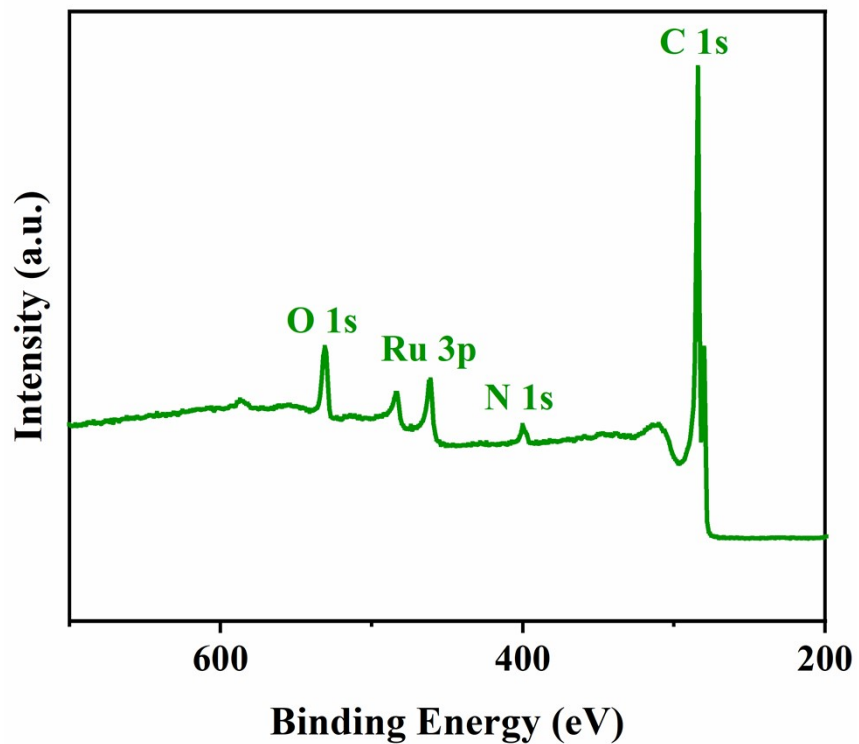


Figure S17. XPS survey scan of Ru/NC.

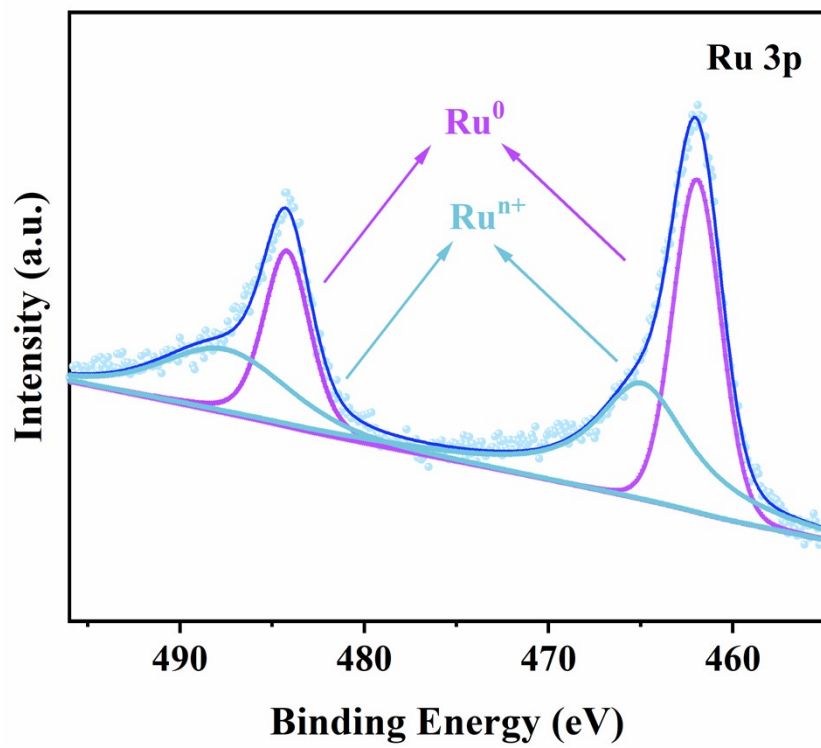


Figure S18. High-resolution XPS spectrum of Ru 3p of Ru/NC.

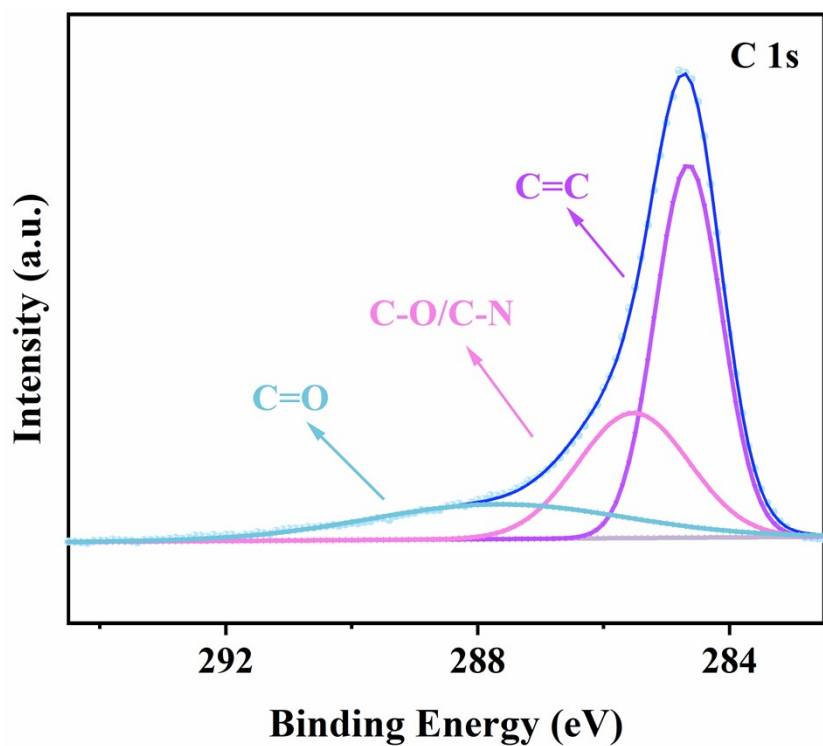


Figure S19. High-resolution XPS spectrum of C 1s of Ru/NC.

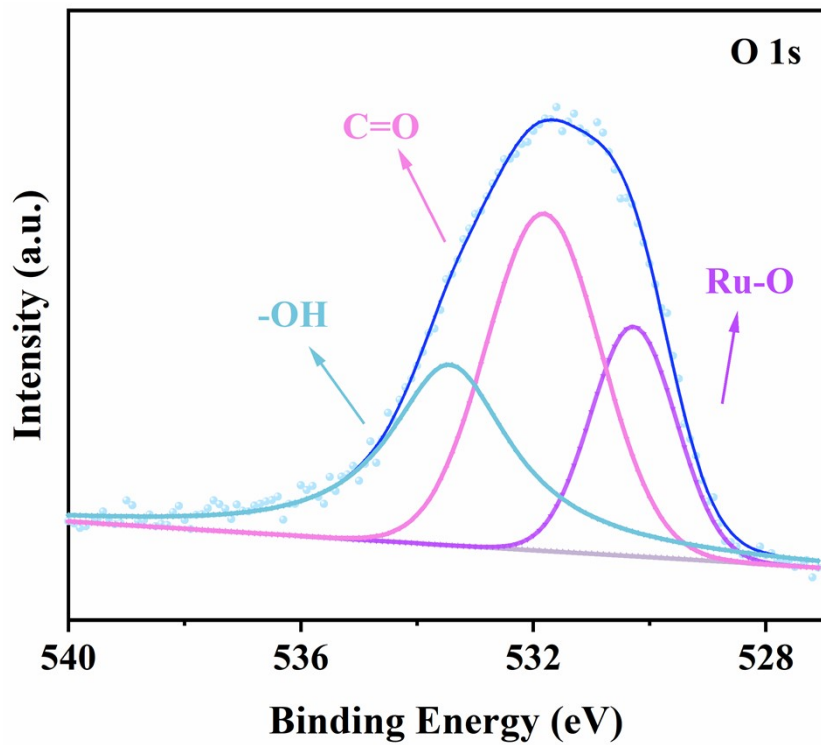


Figure S20. High-resolution XPS spectrum of O 1s of Ru/NC.

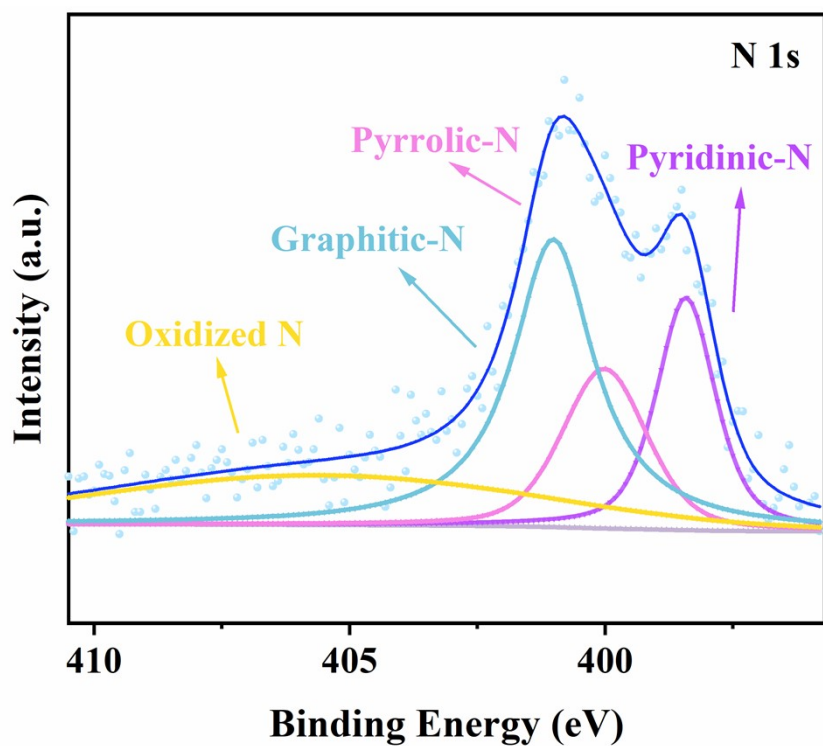


Figure S21. High-resolution XPS spectrum of N 1s of Ru/NC.

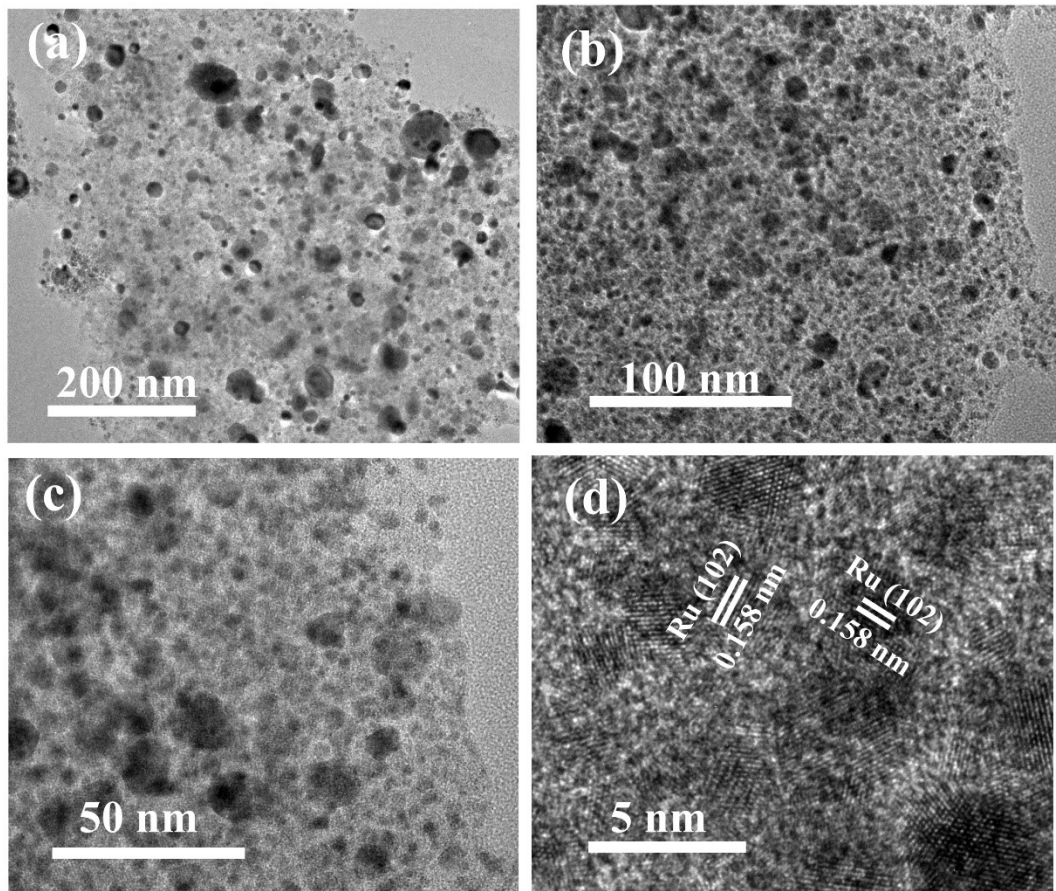


Figure S22. TEM images of Ru/NC under different magnifications.

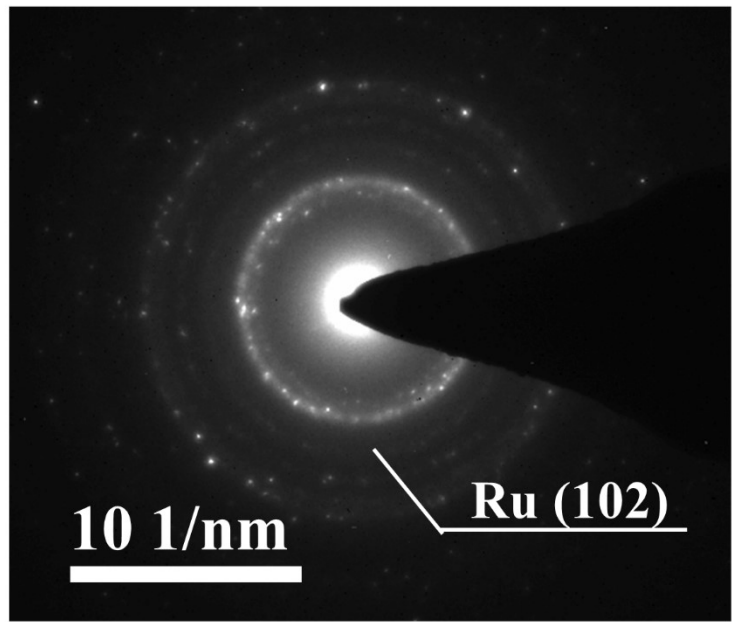


Figure S23. The SEAD pattern recorded from the corresponding area.

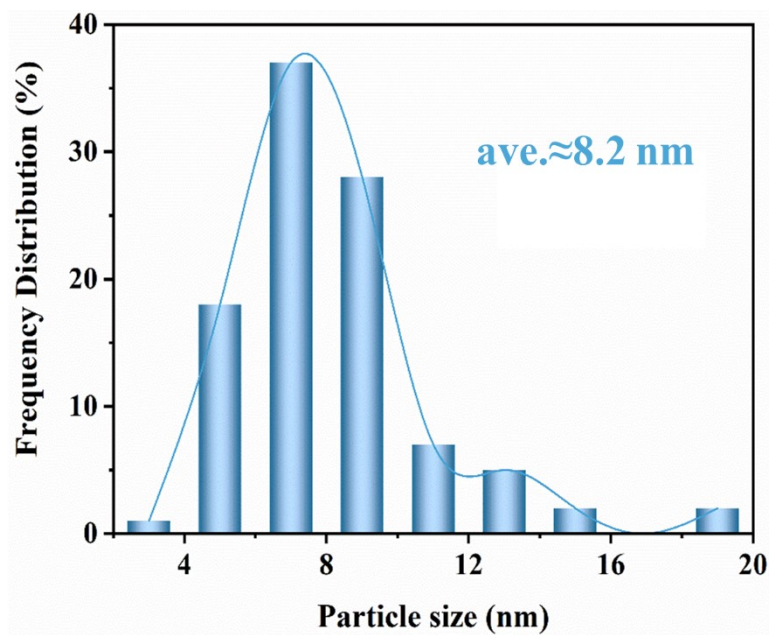


Figure S24. Size distribution histogram of Ru nanoparticles for Ru/NC.

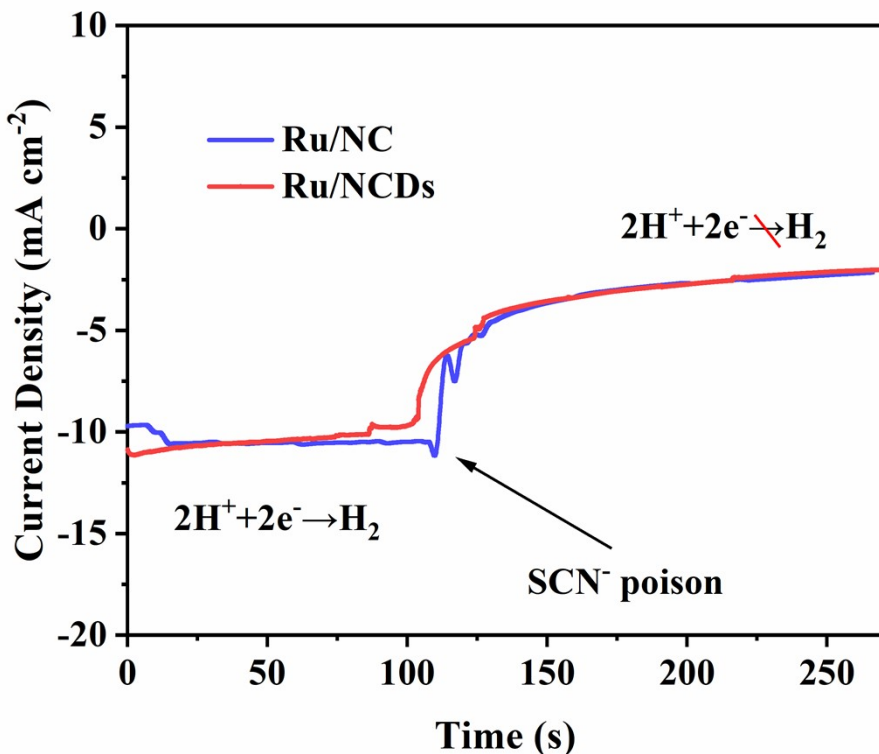


Figure S25. Current-time curves of Ru/NCDs and Ru/NC before and after the addition of SCN⁻ ions in 0.5 M H₂SO₄ solution.

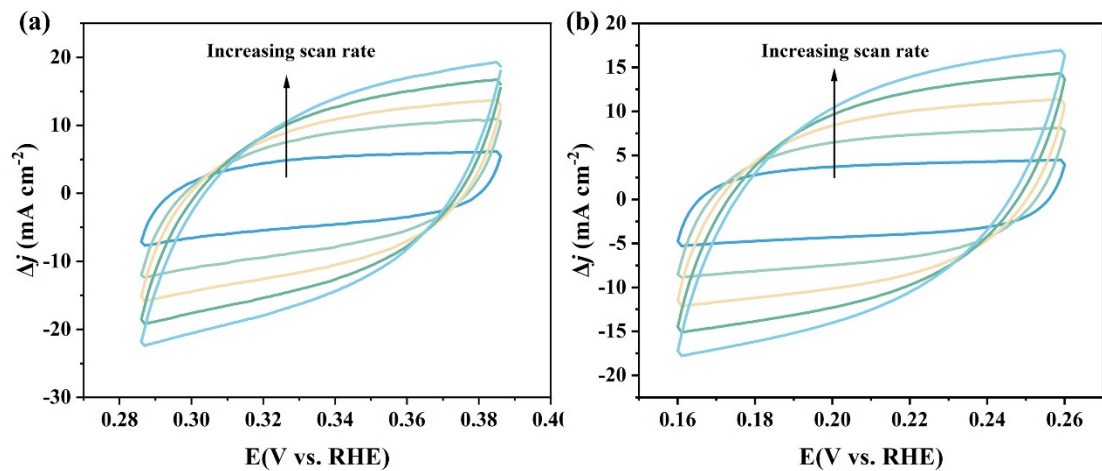


Figure S26. CV curves of Ru/NCDs. Scan rates: 20, 40, 60, 80, 100 $\text{mV}\cdot\text{s}^{-1}$ in (a) 1.0 M KOH and (b) 0.5 M H_2SO_4 solutions.

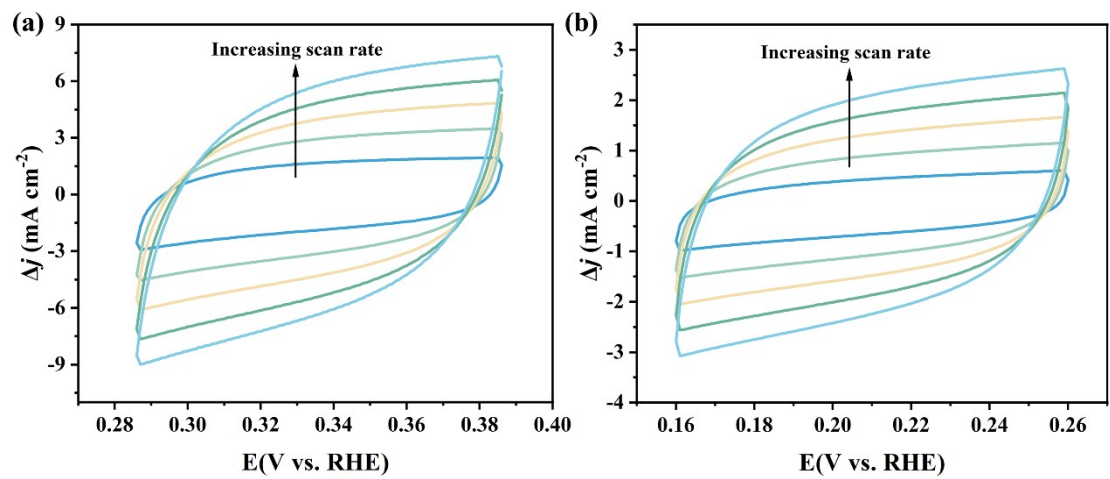


Figure S27. CV curves of Ru/NC. Scan rates: 20, 40, 60, 80, 100 $\text{mV}\cdot\text{s}^{-1}$ in (a) 1.0 M KOH and (b) 0.5 M H_2SO_4 solutions.

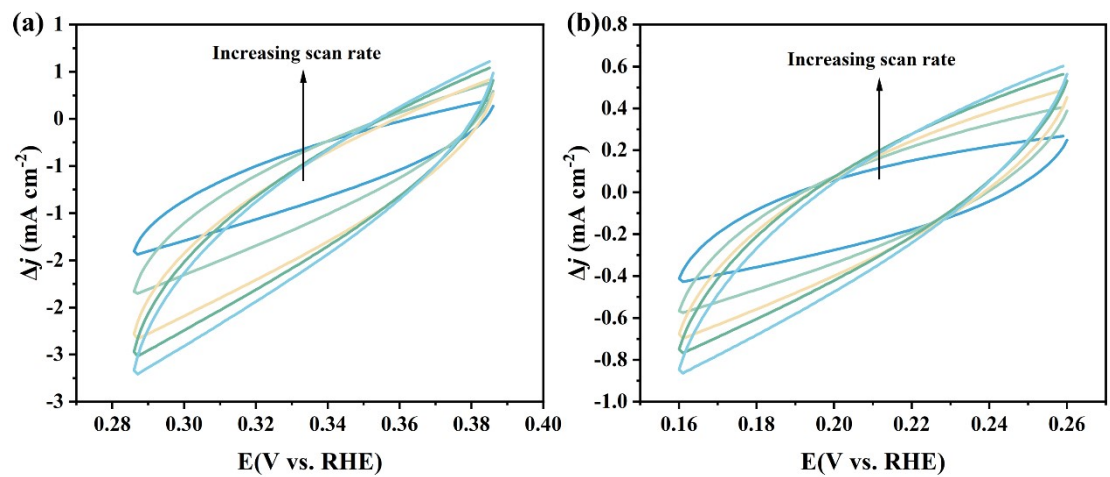


Figure S28. CV curves of NCDs. Scan rates: $20, 40, 60, 80, 100\text{ mV}\cdot\text{s}^{-1}$ in (a) 1.0 M KOH and (b) $0.5\text{ M H}_2\text{SO}_4$ solutions.

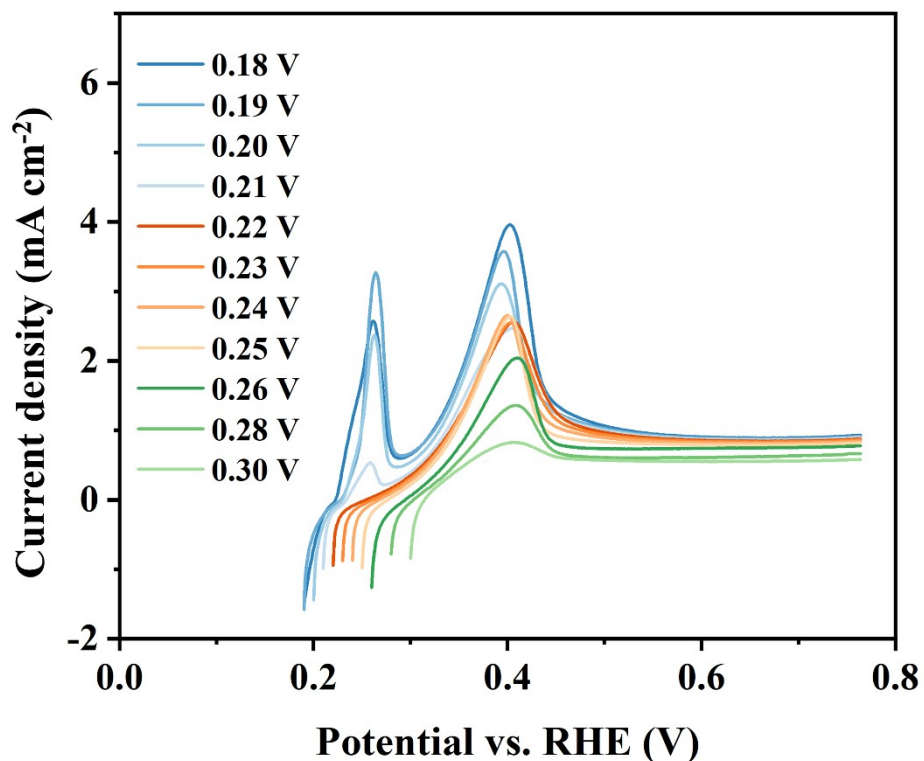


Figure S29. The linear sweep voltammetry (LSV) curves for the stripping of Cu deposited at different overpotentials from 0.18 to 0.3 V in a 0.5 M H_2SO_4 + 20 mM CuSO_4 + 60 mM NaCl solution (scan rate of 2 mVs^{-1}).

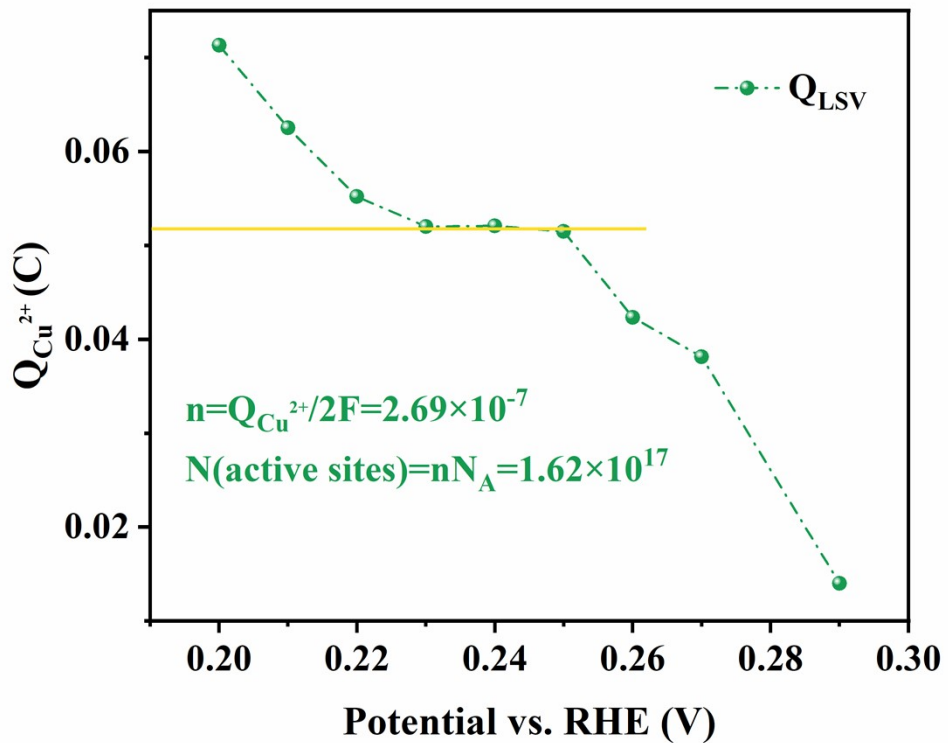


Figure S30. The charges required to strip the Cu deposited at different underpotentials in Ru/NC.

Table S1. The Bader charge analysis of Ru/NCDs.

Ru atom	Δq
Ru (near-neighboring carbon layer)	-0.22801
Ru (near-neighboring carbon layer)	-0.26113
Ru (near-neighboring carbon layer)	-0.26924
Ru (near-neighboring carbon layer)	-0.1946
Ru (next-neighboring carbon layer)	0.050826
Ru (next-neighboring carbon layer)	0.103153

Table S2. Comparison of recently reported electrocatalysts for HER in 0.5 M H₂SO₄.

Catalyst	Overpotential at 10 mA cm ⁻² (mV)	Tafel slope (mV dec ⁻¹)
This work	15	25
Ru/C ¹	35	36.2
Ru ⁰ /TiO ₂ ²	41	52
Ru ₁ CoP/CDs ³	49	51.6
Ru@NO-C ⁴	172	38.9
Ru@C ₂ N ⁵	13.5	30
Ru-MoO ₂ ⁶	55	44
Ru@NG ⁷	42.7	55
Ru _{2.0} /HNCS ⁸	39	30
Ni@Ni ₂ P-Ru ⁹	51	35
Ru-NC-700 ¹⁰	29	28
0.27- RuO ₂ @C ¹¹	33	53
RuP (L-RP) ¹²	19	37
Ru-NGC ¹³	25	31
RuP ₂ @NPC ¹⁴	38	38
Cu _{2-x} @Ru NPs ¹⁵	129	65
Ru@CNF ¹⁶	55	27.19
NiRu@N-C ¹⁷	50	36

Table S3. The fitted parameters of the EIS data of different catalysts for HER in 0.5 M H₂SO₄.

Catalysts	Rs (Ω)	T (F sn-1)	R1 (Ω)	R2 (Ω)	Cφ (F)
Ru/NCDs	7.691	6.759E-001	5.195	2.275	2.559E-003
Ru/NC	6.316	5.716E-001	9.881	9.413	6.665E-004
Ru NPs	8.832	4.651E-001	13.42	33.91	1.035E-003
NCDs	7.086	4.583E-001	171	233.1	2.676E-004
NC	6.234	8.757E-001	823.6	744.9	4.016E-004

Table S4. The fitted parameters of the EIS data of different catalysts for HER in 1.0 M KOH.

Catalysts	Rs (Ω)	T (F sn-1)	R1 (Ω)	R2 (Ω)	C ϕ (F)
Ru/NCDs	7.647	6.601E-001	5.302	2.511	3.348E-003
Ru/NC	6.693	4.339E-001	9.715	12.75	8.831E-004
Ru NPs	8.224	6.887E-001	193	140.7	5.219E-004
NCDs	8.951	8.779E-001	653.8	679.6	1.047E-005
NC	8.851	8.617E-001	733.1	644.4	9.795-006

Table S5. Comparison of the recently reported Ru-based electrocatalysts for HER in 1.0 M KOH.

Catalyst	Overpotential at 10 mA cm ⁻² (mV)	Tafel slope (mV dec ⁻¹)
This work	31	22
Ru/C ¹	53	36.2
RuCu/C ¹⁸	43.4	49
Ru _{2.0} /HNCS ⁸	72	67
Ru@NG-750 ¹⁹	40	35.9
Ru@CQDs ²⁰	63	63
Au–Ru NWs ²¹	50	30.8
Ru ₂ P@PNC/CC ²²	50	66
RuP ₂ /NPG ¹⁴	52	69
Ni@Ni ₂ P-Ru ⁹	41	31
(Ru-Co)O _x /CC ²³	44.1	23.5
Ru-NGC ¹³	37	40
Ru-Ni@Ni ₂ P-HNRs ⁹	31	41
Ru _{0.33} Se@ TNA ²⁴	57	50
Cu _{2-x} @Ru NPs ¹⁵	82	48
Ru@CN ²⁵	32	53
NiRu@N-C ¹⁷	32	64
h-RuSe ₂ ²⁶	34	95

Table S6. TOF value of Ru/NCDs and Ru/NC in 1.0 M KOH at different potentials.

Potential (mV)	TOF value of Ru/NCDs (H ₂ s ⁻¹)	TOF value of Ru/NC (H ₂ s ⁻¹)
10	0.06001	0.08123
20	0.06675	0.08638
30	0.13918	0.09497
40	0.35936	0.15461
50	0.55797	0.26215
60	0.74126	0.38611
70	0.92029	0.51836
80	1.11928	0.64542
90	1.26154	0.77031
100	1.37775	0.87856

Table S7. TOF value of Ru/NCDs and Ru/NC in 0.5 M H₂SO₄ at different potentials.

Potential (mV)	TOF value of Ru/NCDs (H ₂ s ⁻¹)	TOF value of Ru/NC (H ₂ s ⁻¹)
10	0.07425	0.03312
20	0.22651	0.09488
30	0.44674	0.20801
40	0.71889	0.34792
50	0.97294	0.50035
60	1.15197	0.65414
70	1.40749	0.80902
80	1.71955	0.95681
90	1.89877	1.11796
100	2.0318	1.27038

Supplementary Note 1

According to prior research,^{27, 28} the Ru/NCDs HER pathway is defined by the following equations:



Three main stages have been experienced: (1) A hydrogen ion adsorbed on the Ru surface combines with an electron to form an adsorbed H atom. (2) Due to the spillover effect, the neutral adsorbed-H atom moves to the NCDs surface. (3) The transferred H atom combines a hydrogen ion and an electron and releases hydrogen gas.

It is generally believed that the third step (S3) is the rate-determining step (rds). The reaction velocity of hydrogen evolution can be written as:

$$r_3 = K_3 a_{H^+},$$

where r_3 is the reaction rate; K_3 is the rate constant; a_{H^+} is the activity of hydrogen ions which can be written as $a_{H^+} = \theta_{Ru-NCDs-H} C_{H^+}$, where $\theta_{Ru-NCDs-H}$ is the coverage of H on carbon; C_{H^+} is the concentration of hydrogen ion.

In the steady state, for $\theta_{Ru-NCDs-H}$

$$\begin{aligned}
& \frac{d\theta_{Ru-NCDs-H}}{dt} \\
&= K_2\theta_{H-Ru-NCDs}(1-\theta_{Ru-NCDs-H}) - K_{-2}\theta_{Ru-NCDs-H}(1-\theta_{H-Ru-NCDs}) \\
&\quad - K_3\theta_{Ru-NCDs-H}C_H +
\end{aligned}$$

for $\theta_{H-Ru-NCDs}$

$$\begin{aligned}
& \frac{d\theta_{H-Ru-NCDs}}{dt} \\
&= K_1(1-\theta_{H-Ru-NCDs})C_H - K_{-1}\theta_{H-Ru-NCDs} - K_2\theta_{H-Ru-NCDs}(1-\theta_{H-Ru-NCDs}) \\
&\quad + K_{-2}\theta_{Ru-NCDs-H}(1-\theta_{H-Ru-NCDs})
\end{aligned}$$

$$\frac{d\theta}{dt} = 0$$

At low overpotential, it can be considered that $\frac{d\theta}{dt} = 0$,

$$\begin{aligned}
& \theta_{Ru-NCDs-H} \\
& \approx \frac{K_2\theta_{H-Ru-NCDs}}{K_2\theta_{H-Ru-NCDs} + K_{-2} - K_{-2}\theta_{H-Ru-NCDs} + K_3C_H} \approx \frac{K_2\theta_{H-Ru-NCDs}}{K_2\theta_{H-Ru-NCDs} + K_{-2} - K_{-2}\theta_{H-Ru-NCDs} + K_3C_H} \\
& e^{-\frac{F\eta}{RT}}
\end{aligned}$$

In which $K_2 = K_2^0 e^{-\frac{\alpha F\eta}{RT}}$ and $K_{-2} = K_{-2}^0 e^{-\frac{(1-\alpha)F\eta}{RT}}$, η is the overpotential.

in the same way,

$$\begin{aligned}
& \theta_{H-Ru-NCDs} \\
& \approx \frac{K_1C_H + K_{-2}\theta_{Ru-NCDs-H}}{K_1C_H + K_{-1} + K_2 + K_{-2}\theta_{Ru-NCDs-H} - K_2\theta_{Ru-NCDs-H}} \\
& r_3 = K_3\theta_{Ru-NCDs-H}C_H = \frac{K_1^0 K_2^0 K_3^0}{K_{-1}^0 K_{-2}^0} (C_H)^2 e^{-\frac{(2+\alpha)F\eta}{RT}}
\end{aligned}$$

Then,

$$-j = Fr = F \frac{K_1^0 K_2^0 K_3^0}{K_{-1}^0 K_{-2}^0} (C_{H^+})^2 e^{-\frac{(2+\alpha)F\eta}{RT}}$$

And,

$$\lg(-j) = Const + 2\lg C_{H^+} - \frac{(2+\alpha)F}{2.303RT}\eta$$

$$\frac{(2+\alpha)F}{2.303RT} = 0.024 mV/dec$$

Therefore, the Tafel slope is $0.024 mV/dec$ (assuming $\alpha = 0.5$)

References

1. Y. Li, J. Abbott, Y. Sun, J. Sun, Y. Du, X. Han, G. Wu and P. Xu, *Appl. Catal. B*, 2019, **258**, 117952.
2. E. Demir, S. Akbayrak, A. M. Onal and S. Ozkar, *J. Colloid Interface Sci.*, 2018, **531**, 570-577.
3. Y. Liu, X. Li, Q. Zhang, W. Li, Y. Xie, H. Liu, L. Shang, Z. Liu, Z. Chen, L. Gu, Z. Tang, T. Zhang and S. Lu, *Angew. Chem. Int. Ed.*, 2020, **59**, 1718-1726.
4. G. Meng, H. Tian, L. Peng, Z. Ma, Y. Chen, C. Chen, Z. Chang, X. Cui and J. Shi, *Nano Energy*, 2021, **80**, 105531.
5. J. Mahmood, F. Li, S. M. Jung, M. S. Okyay, I. Ahmad, S. J. Kim, N. Park, H. Y. Jeong and J. B. Baek, *Nat. Nanotechnol.*, 2017, **12**, 441-446.
6. P. Jiang, Y. Yang, R. Shi, G. Xia, J. Chen, J. Su and Q. Chen, *J. Mater. Chem. A*, 2017, **5**, 5475-5485.
7. J. Yang, H. Guo, S. Chen, Y. Li, C. Cai, P. Gao, L. Wang, Y. Zhang, R. Sun, X. Niu and Z. Wang, *J. Mater. Chem. A*, 2018, **6**, 13859-13866.
8. A. Jiang, Z. Wang, Q. Li and M. Dong, *Mater. Today Phys.*, 2021, **16**, 100300.
9. Y. Liu, S. Liu, Y. Wang, Q. Zhang, L. Gu, S. Zhao, D. Xu, Y. Li, J. Bao and Z. Dai, *J. Am. Chem. Soc.*, 2018, **140**, 2731-2734.
10. B. Lu, L. Guo, F. Wu, Y. Peng, J. E. Lu, T. J. Smart, N. Wang, Y. Z. Finfrock, D. Morris, P. Zhang, N. Li, P. Gao, Y. Ping and S. Chen, *Nat. Commun.*, 2019, **10**, 631.
11. H.-S. Park, J. Yang, M. K. Cho, Y. Lee, S. Cho, S.-D. Yim, B.-S. Kim, J. H. Jang

- and H.-K. Song, *Nano Energy*, 2019, **55**, 49-58.
12. J. Yu, Y. Guo, S. She, S. Miao, M. Ni, W. Zhou, M. Liu and Z. Shao, *Adv. Mater.*, 2018, **30**, e1800047.
13. Q. Song, X. Qiao, L. Liu, Z. Xue, C. Huang and T. Wang, *Chem. Commun.*, 2019, **55**, 965-968.
14. Z. Pu, I. S. Amiinu, Z. Kou, W. Li and S. Mu, *Angew. Chem. Int. Ed.*, 2017, **56**, 11559-11564.
15. D. Yoon, J. Lee, B. Seo, B. Kim, H. Baik, S. H. Joo and K. Lee, *Small*, 2017, **13**, 1700052.
16. Q. Xie, Z. Wang, L. Lin, Y. Shu, J. Zhang, C. Li, Y. Shen and H. Uyama, *Small*, 2021, **17**, e2102160.
17. Y. Xu, S. Yin, C. Li, K. Deng, H. Xue, X. Li, H. Wang and L. Wang, *J. Mater. Chem. A*, 2018, **6**, 1376-1381.
18. K. Gao, Y. Wang, Z. Wang, Z. Zhu, J. Wang, Z. Luo, C. Zhang, X. Huang, H. Zhang and W. Huang, *Chem. Commun.*, 2018, **54**, 4613-4616.
19. L. Bai, Z. Duan, X. Wen, R. Si, Q. Zhang and J. Guan, *ACS Catal.*, 2019, **9**, 9897-9904.
20. W. Li, Z. Wei, B. Wang, Y. Liu, H. Song, Z. Tang, B. Yang and S. Lu, *Mater. Chem. Front.*, 2020, **4**, 277-284.
21. Q. Lu, A. L. Wang, Y. Gong, W. Hao, H. Cheng, J. Chen, B. Li, N. Yang, W. Niu, J. Wang, Y. Yu, X. Zhang, Y. Chen, Z. Fan, X. J. Wu, J. Chen, J. Luo, S. Li, L. Gu and H. Zhang, *Nat. Chem.*, 2018, **10**, 456-461.

22. T. Liu, B. Feng, X. Wu, Y. Niu, W. Hu and C. M. Li, *ACS Appl. Energy Mater.*, 2018, **1**, 3143-3150.
23. C. Wang and L. Qi, *Angew. Chem. Int. Ed.*, 2020, **59**, 17219-17224.
24. K. Wang, Q. Chen, Y. Hu, W. Wei, S. Wang, Q. Shen and P. Qu, *Small*, 2018, **14**, e1802132.
25. J. Wang, Z. Wei, S. Mao, H. Li and Y. Wang, *Energy Environ. Sci.*, 2018, **11**, 800-806.
26. Y. Zhao, H. Cong, P. Li, D. Wu, S. Chen and W. Luo, *Angew. Chem. Int. Ed.*, 2021, **60**, 7013-7017.
27. Y. Cheng, S. Lu, F. Liao, L. Liu, Y. Li and M. Shao, *Adv. Funct. Mater.*, 2017, **27**, 1700359.
28. L. Zhu, H. Lin, Y. Li, F. Liao, Y. Lifshitz, M. Sheng, S. T. Lee and M. Shao, *Nat. Commun.*, 2016, **7**, 12272.